SISSA ISAS

FERMILAB

LIBRARY

SISSA-119-95-A

Fermilab Library 0 1160 0050383 3

Reconstructing Positions & Velocities of Galaxy Clusters within 20000 km/sec. I: The Cluster 3D Dipole

Enzo BRANCHINI[1] & Manolis PLIONIS[1,2]

[1] SISSA-*International School for Advanced Studies*, Via Beirut 2-4, 34013 Trieste, Italy SISSA, Trieste

[2] *National Observatory of Athens*, Lofos Nimfon, Thesio 11810, Athens, Greece

Athens Observatory

Abstract

Starting from the observed distribution of Abell/ACO galaxy clusters in redshift space we use a two–step procedure to recover their distances and peculiar velocities. After statistically correcting for the unobserved cluster distribution in the zone of avoidance and also for a smooth absorption at higher latitudes, we use a dynamical iterative algorithm, based on that of Strauss & Davis (1988), to recover the real–space cluster positions by minimizing the redshift space distortions. The whole procedure assumes that clusters trace the mass, that peculiar velocities are caused by gravity and that linear perturbation theory applies. The amplitude of the cluster dipole measured in the 3D space turns out to be $\sim 23\%$ less than that measured in redshift space. In both cases the dipole direction is aligned with the Cosmic Microwave Background dipole within $\sim 10°$, taking into account the Virgocentric infall component of the Local Group motion. Using linear theory we obtain $\beta_c(\equiv \Omega_o^{0.6}/b_c) \approx 0.21(\pm 0.03)$, where the uncertainty is due to observational errors and limitations in the reconstruction procedure while the intrinsic cosmological variance amounts to ~ 0.07 . This β_c value implies that for a cluster–mass bias parameter of $b_c \lesssim 5$, a flat Universe is not excluded, contrary to previous cluster-dipole z-space analysis. A more stringent determination of β_c will be obtained from the analysis of the peculiar velocity field in a forthcoming paper.

ApJ in press

SISSA ref. 119/95/A

Via Beirut 2-4 - 34014 Trieste - ITALY

ABSTRACT

Starting from the observed distribution of Abell/ACO galaxy clusters in redshift space we use a two–step procedure to recover their distances and peculiar velocities. After statistically correcting for the unobserved cluster distribution in the zone of avoidance and also for a smooth absorption at higher latitudes, we use a dynamical iterative algorithm, based on that of Strauss & Davis (1988), to recover the real–space cluster positions by minimizing the redshift space distortions. The whole procedure assumes that clusters trace the mass, that peculiar velocities are caused by gravity and that linear perturbation theory applies. The amplitude of the cluster dipole measured in the 3D space turns out to be $\sim 23\%$ less than that measured in redshift space. In both cases the dipole direction is aligned with the Cosmic Microwave Background dipole within $\sim 10°$, taking into account the Virgocentric infall component of the Local Group motion. Using linear theory we obtain $\beta_c(\equiv \Omega_o^{0.6}/b_c) \approx 0.21(\pm 0.03)$, where the uncertainty is due to observational errors and limitations in the reconstruction procedure while the intrinsic cosmological variance amounts to ~ 0.07 . This β_c value implies that for a cluster–mass bias parameter of $b_c \lesssim 5$, a flat Universe is not excluded, contrary to previous cluster-dipole z-space analysis. A more stringent determination of β_c will be obtained from the analysis of the peculiar velocity field in a forthcoming paper.

Subject headings: cosmology: observations – galaxies: clustering – galaxies: distances and redshifts – large-scale structure of universe

1. Introduction

The best evidence that cosmic structures can have significant velocities, above their cosmological expansion velocities, came from the interpretation of the CMB temperature dipole anisotropy as a Doppler effect, originating from the motion, with $v_{LG} = 622 \pm 20$ km/sec, of the Local Group of galaxies (LG hereafter) in the isotropic CMB radiation sea, towards $l = 277°$ and $b = 30°$ (Lubin & Villela 1986; Kogut et al. 1993)

If linear gravity is responsible for the observed peculiar velocities then according to the linear gravitational instability theory (cf. Peebles 1980) the peculiar gravitational acceleration should be aligned and proportional to the peculiar velocity; the constant of proportionality being a measure of the present-time growth rate of mass fluctuations and therefore a measure of the cosmological density parameter, Ω_o. The gravitational acceleration of an extragalactic object can be estimated by calculating the dipole moment of the distribution of mass surrounding it. Since, however, the latter is unknown one has to resort in estimating the dipole moment of the distribution of luminous extragalactic objects using some simplifying assumption about the relation between fluctuations in the matter and light distributions; which usually is non other than the *linear-biasing* assumption (cf. Kaiser 1984). In this picture the galaxy fluctuations, δ_g, are related to those of the matter distribution δ by a constant factor, the biasing parameter, $\delta_g = b\delta$.

Further difficulties arise from the fact that one can observe galaxies or other extragalactic objects limited in magnitude or flux, which then implies that distant contributions to the dipole could be missed if the characteristic depth of the galaxy catalogue is less than the convergence depth of the dipole. Moreover, most catalogues of extragalactic objects have also limited sky coverage which is usually due to light absorption near the Galactic plane.

Up to now the dipole of various populations of extragalactic objects has been determined: optical galaxies (Lahav 1987; Plionis 1988; Lahav, Rowan-Robinson & Lynden-Bell 1988; Lynden-Bell, Lahav & Burstein 1989; Hudson 1993b), IRAS galaxies (Meiksin & Davis 1986; Yahil, Walker & Rowan-Robinson 1986; Villumsen & Strauss 1987; Strauss & Davis 1988; Strauss et al. 1992; Rowan-Robinson et al. 1990; Plionis, Coles & Catelan 1993), X-ray active galactic nuclei (Miyaji & Boldt 1990); X-ray clusters (Lahav et al. 1989) and Abell clusters (Scaramella, Vettolani & Zamorani 1991 [hereafter SVZ91]; Plionis & Valdarnini 1991 [hereafter PV91]). In all cases the dipole moment was found to be well aligned with the CMB dipole suggesting that gravity is indeed responsible for the Local Group motion and that light traces mass.

An interesting historical fact, originating from these studies, is that the estimated dipole convergence depth has been a function of cosmic volume sampled; *the deeper the catalogue the larger the dipole convergence depth.* This is true out to the largest depths, traced by the Abell/ACO cluster catalogue, for which $R_{conv} \approx 17000$ km/sec (PV91 and SVZ91). This implies that the apparent

dipole convergence of the shallower galaxy catalogues (being optical or IRAS) is probably artificial, determined by their limiting depth. In fact a careful investigation of the QDOT-IRAS sample provided some evidence for a contribution to the dipole from scales comparable to the cluster R_{conv} (Plionis, Coles & Catelan 1993; Plionis 1995). Furthermore, a simulation based study did indeed show that if contributions to the LG exist from depths comparable to the cluster R_{conv}, then the IRAS 0.6 Jy selection function is such that the IRAS dipole would be underestimated by on average 15% - 20%(Kolokotronis et al. 1995).

A further interesting outcome of the Abell/ACO cluster dipole analysis is the fact that there seems to be a *coherent* dipole anisotropy out to $\sim$ 17000 km/sec; i.e., the differential gravitational acceleration induced on the Local Group by the distribution of clusters in large equal-volume shells is roughly aligned with the CMB dipole in each shell (PV91). Furthermore, there is strong evidence for the existence of coherent large-scale galaxy flows in the local Universe, extending from the Perseus-Pisces region on the one side to the Hydra-Centaurus/Great Attractor region on the other. These flows are well established both for elliptical (cf. Lynden-Bell et al. 1988) and spiral galaxies (cf. Rubin et al. 1976; Dressler & Faber 1990; Mould et al. 1991; Willick 1990; Han & Mould 1990; Courteau et al. 1993; Hudson 1994; Mathewson & Ford 1994) and point in the general direction of the CMB dipole. These results put together present a consistent picture in which the LG participates in a large-scale bulk motion induced by gravity, encompassing a large volume of radius $\sim 6000 - 15000$ km/sec (for recent reviews see Dekel 1994 and Strauss & Willick 1995).

This picture has been recently challenged by Lauer & Postman (1994) [hereafter LP94] who have extended the cosmic flow studies to very large scales, those traced by galaxy clusters, and who find that the LG motion with respect to the frame defined by Abell/ACO clusters, within 15000 km/sec, moves in a direction very different than that of the CMB dipole which then implies that, if the CMB dipole is a Doppler effect, the whole cluster frame is moving with respect to the CMB rest-frame with $\sim$ 700 km/sec. Such a large velocity on such large scales is in contradiction with most theories of structure formation (cf. Strauss et al. 1994; Feldman & Watkins 1994; but see Jaffe & Kaiser 1994). Furthermore, the LP94 result puts into doubt the gravitational instability scenario, for the origin of cosmic structure, because on the scales traced by galaxy clusters linear theory should apply, in which velocity and acceleration are aligned and as mentioned before, the cluster dipole (acceleration) is indeed very well aligned ($\delta\theta_{cmb} \leq 15°$) with the CMB dipole (PV91; SVZ91).

So we are left with the following puzzling picture: the acceleration determined from the distribution of galaxies (within $\sim$ 10000 km/sec) and of clusters (within $\sim$ 25000 km/sec) is well aligned with the CMB dipole (which is in itself a strong indication that the CMB dipole is Doppler generated) while the LG velocity (as determined by LP94), with respect to the cluster frame within 15000 km/sec, points to a direction almost perpendicular to the CMB dipole direction. One would then be forced to explain the alignment of the LG gravitational acceleration, determined from

the distribution of clusters and galaxies, with the CMB dipole direction as a *'cosmic'* coincidence. However, the random joint probability of having the cluster dipole, the optical and IRAS galaxy dipoles aligned with the CMB dipole within a few degrees ($\sim 10°$, $\sim 10°$ and $\sim 25°$ respectively), assuming that they are independent, is $\leq 3 \times 10^{-6}$. Furthermore, as we discussed previously, PV91 found evidence for a coherent dipole anisotropy, in which the differential cluster dipole in each equal-volume shell roughly points towards the CMB dipole. In fact, the dipole in the first shell ($R \lesssim 100\ h^{-1}$ Mpc) has $\delta\theta \lesssim 20°$ while in the most distant shell ($140 \lesssim R \lesssim 160\ h^{-1}$ Mpc), for which the dipole is aligned with the CMB, it has $\delta\theta \lesssim 10°$ and the distance between the centers of the two shells is $\sim 90\ h^{-1}$ Mpc, a distance at which $\xi_{cc}(r) \ll 1$, where ξ_{cc} is the spatial cluster–cluster correlation function (note that even the edges of the two shells are $\sim 43\ h^{-1}$ Mpc away). Therefore, these two volumes could be considered independent which would then decrease even further the probability of random alignment with the CMB dipole to $\lesssim 8 \times 10^{-8}$!

We attempt to throw light to this paradox by using linear perturbation theory and a dynamical reconstruction algorithm (based on that of Strauss & Davis 1988) to determine the 3D cosmic density field, traced by the Abell/ACO galaxy clusters within $\lesssim$ 20000 km/sec, with the aim of investigating

1. whether the large cluster-dipole convergence depth, its asymptotic amplitude and the alignment of the z-space cluster dipole with that of the CMB, are artifacts of redshift space distortions,

2. the peculiar velocity field, within 20000 km/sec, as predicted by linear theory and compare it *(a)* to that derived using galaxy samples and *(b)* to the LP94 results.

However, there are a number of possible concerns in using clusters as mass tracers. Firstly, their large relative separation causes them to sparsely trace the mass distribution and therefore they cannot provide information about the small scale density field. Nevertheless, it is exactly this fact that allows linear theory to be applied efficiently. Furthermore, Bachall et al. (1994) have shown, using numerical simulations, that clusters are very efficient tracers of the linear velocity field. The second concern is related to the linear biasing assumption and although there is some physical justification for its use, it is expected to be only a crude approximation to the true relation between the cluster and underline density fields. However, Plionis (1995) and Kolokotronis et al. (1995) provide some recent support for linear biasing between clusters and galaxies on large scales. A third possible problem is the 'zero-point' uncertainty from which the cluster dipole is bound to suffer since nearby Abell-like clusters, like Virgo, are missed in the Abell/ACO catalogue. In this study we do attempt to correct for it but in any case such a problem is local and cannot affect the reconstruction procedure as a whole. Finally we note that, as shown by Scaramella (1995) and in our preliminary analysis (Branchini & Plionis 1995), the use of the Abell/ACO cluster as mass tracers can be convincingly justified also by the agreement *a posteriori*, both quantitative and qualitative, between the galaxy and the cluster velocity and density fields.

In this first paper we will present our method of analysis and we will address the first set of questions, outlined above; while the second will be addressed in a forthcoming paper. The plan of this paper is as follows: In section 2 we present an extended discussion of the two subsamples used, of their biases and homogenization procedure. In section 3 we present both the zone of avoidance *filling* procedure, the dynamical real–space reconstruction algorithm and its reliability tests. In section 4 we present the cluster dipole estimate, possible systematic effects and an extended error analysis. In section 5 we derive interesting cosmological parameters from the dipole analysis and finally in section 6 we present our conclusions.

2. The Cluster Sample

Our present analysis is based on a cluster sample extracted from the original Abell sample (Abell 1958) and from its southern extension, the ACO cluster catalogue (Abell, Corwin & Olowin 1989). The north declination limit of the ACO sample is $\delta = -17$, so that the two catalogues overlap in the strip $-27 \leq \delta \leq -17$. The overlapping region has been used by Abell, Corwin & Olowin (1989) to calibrate the J magnitudes of the ACO to the Abell magnitude system. However, systematic differences in the two calibrated catalogues have been noticed by ACO (1989), Batusky et al. (1989), Scaramella et al. (1990) and PV91 which cannot be ascribed to the suspected incompleteness of the richness class $R = 0$ clusters since the differences are evident, although less pronounced, even in the $R \geq 1$ samples (see PV91 and section 2.2 below).

The problem of obtaining a composite and statistically homogeneous catalogue from the Abell and ACO samples, is particularly important in dipole studies since artificial systematic differences (density gradients or global density variations) can enhance or even produce a dipole signal. Although this issue has been addressed by a number of authors (cf. Scaramella et al. 1990 and PV91) we will also discuss it, following the PV91 line of reasoning.

Cluster distances, r, are estimated from redshifts using the standard relation:

$$r = \frac{c}{H_o q_o^2 (1+z)} \left[q_o z + (1 - q_o) \left(1 - \sqrt{2 q_o z + 1} \right) \right], \tag{1}$$

where c is the speed of the light and q_o the deceleration parameter. The number of clusters within our subsample is not fixed since the distances slightly depend on q_o which we do not fix *a priori*. We also merge cluster pairs with relative distance $\leq 3\ h^{-1}$ Mpc into unique 'clusters' having as position their center of mass and as mass their combined total mass. We made this approximations to avoid nonlinear effects on small scales for which our reconstruction method fails to account for. The combined subsample we consider is composed by:

1. Abell clusters of richness class $R \geq 0$ in the roughly volume–limited region $r \leq 250\ h^{-1}$ Mpc, $|b| \geq 13°$ and with $m_{10} < 17$. m_{10} is the magnitude of the tenth brightest galaxy in the

cluster in the magnitude system corrected according to PV91. This sample is 100 % redshift complete. Note that the number of objects in this subsample varies between 269 and 276 for $q_o = 0.2$ and 0.5, respectively. Out of these we have merged 5 cluster pairs.

2. ACO clusters of richness class $R \geq 0$ with $r \leq 250\ h^{-1}$ Mpc, $|b| \geq 13°$ and $m_{10} < 17$. Among the 217 objects within the sample $\sim$ 77% have measured redshift. For the remaining objects the redshift is determined using the $m_{10} - z$ relation used by PV91. Note that we have merged 7 cluster pairs.

Note that although Abell cautioned that the $R = 0$ cluster sample is not complete and therefore probably not suitable for statistical studies, many recent studies have been interestingly utilizing them (c.f. Tully 1987; Postman et al 1989; Huchra et al. 1990; Tully et al. 1992; Scaramella et al 1994). Furthermore, the density distributions and clustering properties of both the $R = 0$ and $R \geq 1$ Abell samples have been found to be similar out to $z \approx 0.2$ possibly indicating the weakness of such effects (Postman et al. 1992; but see Peacock & West 1992). In any case the stability of our main results as a function of cluster richness will be discussed in the relevant section.

2.1. The Selection Biases

In order to obtain a statistically homogeneous all–sky sample of clusters we quantify separately the observational biases, of the Abell and ACO subsamples, and then we calibrate these subsamples applying a homogenization procedure.

At low galactic latitudes, absorption of optical photons makes it unlikely to observe luminous objects. In the galactic strip $|b| \leq 20°$, to which we refer as the Zone of Avoidance (ZoA), there are only 20 clusters in our subsample. The galactic absorption outside the ZoA has been always found to be consistent with a cosecant law:

$$\log P(b) = \alpha(1 - \mathrm{cosec}|b|), \tag{2}$$

where $P(b)$ gives the probability that a cluster in the range b to $b + \Delta b$ would have been included in the catalogue. There is no general agreement on the precise value of α. Bahcall & Soneira (1983) and Postman et al. (1989) found 0.3 for Abell clusters, Batuski et al. (1989) found $\alpha \sim 0.2$ for ACO clusters while LP94 found an even lower value ($\alpha \sim 0.15$) for both ACO and Abell clusters contained in a volume–limited 15000 km/sec sphere. To allow for this experimental uncertainty we will consider, in what follows, two different sets of values: (α, α)= (0.3,0.2), that better matches the behaviour of the number density of our cluster as a function of the galactic latitude and (0.2,0.2). The first value in each set refers to the Abell sample while the second to the ACO one.

The finite depth of the cluster sample was modeled with the redshift selection function that was estimated as in Postman et al. (1989). We modeled the probability that a cluster in the range z to

$z + \Delta z$ would have been included in the cluster catalogue as:

$$P(z) = \begin{cases} 1 & \text{if } z \leq z_c \\ A \exp(-z/z_o) & \text{if } z > z_c \end{cases} \tag{3}$$

where z_c is the redshift up to which the space density of clusters remains constant (volume-limited regime). We obtain $z_c \sim 0.0787$ and 0.0664 for the Abell and ACO subsamples respectively. No appreciable declination dependence has been detected in the Abell/ACO subsample (but see Scaramella et al. 1990 for a possible zenithal dependence).

2.2. Homogenization of the Abell/ACO sample

In this work we will follow the PV91 homogenization scheme, used to minimize the density variations of the Abell and ACO subsamples. The estimated observational biases allow us to assign the following weight to clusters:

$$w_i(z, b) = \frac{1}{P(z_i)P(b_i)}. \tag{4}$$

The individual number density of clusters of the two subsamples is therefore $n = V^{-1} \sum_i w_i(z, b)$, where the sum extends over all clusters within the sampled volume V. Since at low galactic latitudes the patchy galactic absorption is not well described by eq.(2) we compute n above $|b| = 30°$. We divided V into equal volume shells with $\delta V \sim 2.6 \times 10^6\ h^{-3}$ Mpc^3 in which we estimated the Abell and ACO cluster number densities separately. Due to the complex geometric boundaries, the volumes were computed by Montecarlo calculations.

Within $\sim 200\ h^{-1}$ Mpc the space densities of the $R \geq 0$ Abell and ACO samples are constant ($P(z) = 1$) with $n \sim 1.6 \pm 0.3 \times 10^{-5}$ and $\sim 2.7 \pm 0.3 \times 10^{-5}\ h^3$ Mpc^{-3}, respectively, while the corresponding values for the $R \geq 1$ samples are $n \sim 8.2 \pm 1.3 \times 10^{-6}$ and $\sim 11 \pm 1.2 \times 10^{-6}\ h^3$ Mpc^{-3}. The scatter was computed from the density fluctuations in the different bins. These values would be reduced by $\sim 18\%$ if no obscuration correction is applied (ie., assuming $P(b) = 1$). Note that although the Abell-ACO density differences are reduced in the $R \geq 1$ sample they are still present, indicating that these density differences are not due to the possible incompleteness of the $R = 0$ clusters (see also Postman et al. 1990; PV91). Furthermore, the Abell-ACO density differences in the richest subsample ($R \geq 2$) are a factor ~ 3 larger even than those of the $R \geq 0$ one.

An approximate homogenization of the two samples was then applied by equating the number density of the two catalogues in each equal volume shell. Assuming that the two catalogues are simply radially inhomogeneous, we computed the following weighting function:

$$\mathcal{W}_{rel}(r) = \begin{cases} 1 & \text{if } \delta \geq -17 \\ \frac{n(r_i, Abell)}{n(r_i, ACO)} & \text{if } \delta < -17 \end{cases} \tag{5}$$

where r_i is the distance of the $i^{\rm th}$ bin. No significant difference was found when using the two different sets of absorption coefficients. Note, however, that this is not the only possible homogenization scheme since we do not know *a priori* which is the true value of the cluster density. We could, therefore, homogenize the two samples by using the inverse of eq.(5), $\mathcal{W}_{rel}(r)^{-1}$. As we will show in section 4 our main results remain stable on the choice of the homogenization scheme.

3. The Reconstruction Method

The whole reconstruction procedure can be schematically represented by the following diagram:

$$z_{obs} \longrightarrow z_{id} \longrightarrow 3D_{obs}$$

Starting from the observed sky redshift space distribution of galaxy cluster, z_{obs}, we generate a synthetic cluster distribution to account for unobserved clusters. This procedure allows us to reconstruct the whole-sky cluster distribution in the redshift space, z_{id}. An iterative reconstruction algorithm, similar to that proposed by Strauss & Davis (1988), is then applied to minimize the redshift space distortion, allowing us to recover the real–space distribution of the observed clusters $3D_{obs}$ and therefore also their peculiar velocities. The *intrinsic* reliability of the entire procedure has been tested using a simulated catalogue of clusters kindly provided to us by S.Borgani.

3.1. z-Space reconstruction scheme

To reconstruct the whole-sky redshift space cluster distribution, z_{id}, we adopted a phenomenological approach. The basic idea is to fill the artificially (due to Galactic absorption) low density regions of the surveyed volume with a synthetic cluster population having the same clustering properties as the distribution of the real clusters and then generate many Monte-Carlo realizations of this population. To this end we divide our procedure into two steps; one to reconstruct the cluster density field above $|b| = 20°$ and one to *fill* the ZoA.

3.1.1. $|b| > 20°$

The first step is to recover the cluster distribution for $|b| > 20°$. We divided our volume into two regions: an inner sphere with a radius of R_{in}=200 h^{-1} Mpc, which we consider as the region of reliable determination of the cluster density field, and an external region $R_{in} < r < 250\ h^{-1}$ Mpc.

In the inner part, in which $P(z) \simeq 1$, we used a Montecarlo rejection method to generate a population of synthetic clusters distributed according to the adopted $P(b)$ probability function and

weighted them by $1/P(z)$ with the further constraint of being *spatially clustered around the real clusters* according to the observed spatial cluster–cluster correlation function (cf. Bahcall & Soneira 1983; Postman et al. 1992; Plionis, Valdarnini & Jing 1992). The following weights are then assigned both to real and mock 1:

$$\tilde{w}_i(r) = \frac{\mathcal{W}_{rel}(r_i)}{P(z_i)}, \tag{6}$$

Finally, the total number of synthetic clusters outside the ZoA is determined by requiring the overall number density of clusters to match the observed number density

$$\tilde{n} = \frac{1}{V}\sum_i \tilde{w}_i(z,b), \tag{7}$$

where $\tilde{w}_i(z,b) = \mathcal{W}_{rel}(r_i)w_i(z,b)$. Beyond 200 h^{-1} Mpc the radial selection function, mainly for the ACO sample, falls below one roughly exponentially causing the simple $1/P(z)$ weighting to generate non negligible shot noise errors. To avoid this problem we reconstructed the cluster distribution in the external regions as follows: the mock cluster distribution was Montecarlo generated to account for the $P(b)$ selection function but *with no spatial correlation with real clusters.* Then, instead of weighting them by $1/P(z)$, for each synthetic objects we generated $1/P(z)$ mock clusters at the same galactic latitude as the parent object but at a randomly chosen galactic longitude. Finally, the actual number of clusters in the outer region has been adjusted by adding or subtracting a few clusters at random until the cluster number density in the external region equates $\tilde{n}$.

3.1.2. Filling the ZoA

The second step is to fill the ZoA. The method we used is close to that proposed by S. Faber and used by Yahil et al. (1991). We divided the equatorial strip $-20° < b < +20°$ into 18 bins of 20° in longitude. In each bin we divided the distance range into bins of 2000 km/sec. The clusters were then sampled in the two northern and southern adjacent strips, defined so that their *joint* solid angle is equal to that of the ZoA. This requirement leads to the following limiting latitude for the strips

$$|b_{lim}| = 90° - \cos^{-1}[2 \times \cos 70°] = 43.16° .$$

The number of synthetic clusters in each ZoA bin was then set equal to the sum of the clusters (real and synthetic) found in the two bins of the northern and southern, adjacent to the ZoA, strips while their position, inside the ZoA bin, was randomly assigned. Finally, the real clusters in the range $13° < |b| < 20°$ are inserted and the total number of synthetic ZoA clusters is adjusted by subtracting a few at random until the average number density of real clusters is reached.

3.1.3. The z_{id} Cluster Distribution

In what follows we will refer to the above 2-step z-reconstruction scheme as the *Randomized Standard Cloned Mask; [RSCM]*. At the end of the whole procedure nearly 50 % of the cluster population is composed by synthetic objects. A typical z_{id} reconstruction is shown in panels (a) and (c) of Figure 1. Black dots represent real clusters while open dots are synthetic objects. The figure displays the projection of the reconstructed cluster distributions onto the supergalactic plane (X_{sup}-Y_{sup} projection; panel a) and orthogonal to it (X_{sup}-Z_{sup} projection; panel c). A simple visual inspection reveals that the synthetic clusters fill the ZoA and smoothly reproduce the clustering observed in the two nearby galactic-latitude strips. Outside the ZoA, as expected, synthetic objects are clustered with the true ones and their density decreases towards the galactic poles.

However, since each cluster has a different weight a more relevant visualization of the z-space cluster distribution is presented as smoothed density maps in panels (b) and (d) where we have overlayed a 20×20 grid (each cell being 2000 km/sec wide) on the cluster distribution of panels (a) and (c) and smoothed the projected distribution using a 2D–Gaussian kernel with $R_{sm} = 1$ cell, while weighting each cluster by $\tilde{w}_i$. What, in fact, we present in these figures is the 'mean' smoothed density field; an average over 10 random realizations of the z-space reconstruction procedure.

3.2. 3D–Space Reconstruction Scheme

Our 3D reconstruction scheme is based on the assumption that the peculiar velocities of clusters are caused by gravitational instability and that linear perturbation theory applies on the scales relevant to the cluster distribution. The distribution of clusters in redshift space differs from the true three–dimensional one by a nonlinear term in the redshift–distance relationship:

$$cz = H_o|\mathbf{r}| + [\mathbf{u}(\mathbf{r}) - \mathbf{u}(0)] \cdot \frac{\mathbf{r}}{|\mathbf{r}|}, \tag{8}$$

where $\mathbf{r}$ is the position of the generic cluster, $\mathbf{u}(\mathbf{r})$ its peculiar velocity, $\mathbf{u}(0)$ the peculiar velocity of the observer placed at the centre of the coordinate system and H_o is the Hubble parameter.

3.2.1. Linear Theory

In linear theory the peculiar velocities are proportional to the peculiar acceleration (cf. Peebles 1980)

$$\mathbf{u}(\mathbf{r}) = \frac{H_o f(\Omega_o)}{4\pi} \int \delta(\grave{\mathbf{r}}) \frac{\grave{\mathbf{r}} - \mathbf{r}}{|\grave{\mathbf{r}} - \mathbf{r}|^3} d^3\grave{r}\ , \tag{9}$$

where $\delta(\mathbf{r}) = [\rho(\mathbf{r}) - \rho_b]/\rho_b$ is the mass density fluctuation about the mean ρ_b, $f(\Omega_o) \simeq \Omega_o^{0.6}$ and Ω_o is the cosmological density parameter at the present epoch. We assume that cluster density fluctuations are related to the mass fluctuations by a constant linear biasing factor:

$$\delta_c(\mathbf{r}) = b_c \delta(\mathbf{r}), \tag{10}$$

where b_c is the bias parameter of clusters with respect to the mass. We can therefore replace $\delta(\mathbf{r})$ with $\delta_c(\mathbf{r})$ in eq.(9) provided that we substitute $f(\Omega_o)$ with $\Omega_o^{0.6}/b_c$ ($\equiv \beta_c$)

In order to apply linear theory we need to smooth the discrete cluster density field on an appropriate scale, where non-linear effects could be important. Since we are using galaxy clusters to probe the density and the peculiar velocity fields, a natural smoothing scale, large enough for linear theory to be valid, would be the cluster correlation length (i.e. the distance r_o at which the spatial cluster–cluster correlation function is unity). Recently Croft & Efstathiou (1994), analysing large N-body simulations, found that the velocity fields traced by galaxy clusters are highly non-linear below $\sim 10\ h^{-1}$ Mpc. Therefore we allow the smoothing radius to vary in the range [10, 30] h^{-1} Mpc. Although the cluster peculiar velocity field, the analysis of which will be presented in a forthcoming paper, does depend on the choice of the smoothing length, the dipole parameters depend only weakly on its choice, as we will see below.

The discrete cluster distribution was smoothed with a top hat window function which is equivalent to smooth the peculiar acceleration with:

$$W(|\grave{\mathbf{r}} - \mathbf{r}|) = \begin{cases} \frac{|\grave{\mathbf{r}}-\mathbf{r}|}{R_{sm}^3} & \text{if } |\grave{\mathbf{r}} - \mathbf{r}| < R_{sm} \\ 1 & \text{if } |\grave{\mathbf{r}} - \mathbf{r}| \geq R_{sm} \end{cases} \tag{11}$$

where R_{sm} is the smoothing length. Since z_{id} is reconstructed up to $R_{max} = 250h^{-1}$ Mpc, the integral in eq.(9) is converted into a sum over all the observed and synthetic clusters within R_{max}:

$$\mathbf{u}(\mathbf{r}) = \frac{\beta_c}{4\pi n_c} \sum_i \left(\frac{M_i}{M_C}\right) W(|\grave{\mathbf{r}} - \mathbf{r}|)\tilde{w}(\grave{\mathbf{r}}_i)\frac{\grave{\mathbf{r}}_i - \mathbf{r}}{|\grave{\mathbf{r}}_i - \mathbf{r}|^3} + \beta_c\frac{\mathbf{r}}{3}\,. \tag{12}$$

The average cluster density n_c is obtained by dividing the average cluster mass density ρ_c with M_C (mass of Coma cluster); ρ_c is given by:

$$\rho_c = \frac{1}{V}\sum_i M_i\tilde{w}(r_i) \tag{13}$$

where M_i is the mass of the generic cluster. As in PV91 and SVZ91 we assume that cluster masses are proportional to the the Abell–catalogue listed number of galaxies per cluster, $M_i \propto N_{A,i}$ (and $N_C = 106$); while the mass of the synthetic clusters was set equal to the average mass of the real clusters. The last term corrects for the net gravity of the homogeneous density background. The correction is necessary since the summation calculates the contribution from the density rather than from overdensity. Eq.(12) measures the true peculiar velocity only if density inhomogeneities outside the surveyed volume can be ignored.

As shown by Vittorio & Juskiewicz (1987) and Juskiewicz, Vittorio & Wyse (1990) in a multipole expansion of the external gravitational field the leading term is the dipole. Its effect is naturally removed if the peculiar velocities are evaluated in the LG frame because the dipole contribution is constant for all objects and does not affect the relative peculiar velocities. The only disadvantage of

the LG frame is that the correction for the solar motion relative to its barycenter is uncertain by $\sim$ 50 - 100 km/sec (Yahil et al. 1977) which, as we will see, is smaller than the errors on the predicted LG velocity. For this reason we used eq.(13) to evaluate the cluster peculiar velocity in the LG frame. The higher order terms in the multipole expansion of the external gravitational field fall off faster than the dipole with distance and are generally negligible for distances smaller than $R_{max}/2$ (Yahil et al. 1991). Possible systematic errors when computing peculiar velocities are therefore expected only at larger distances and should not appreciably affect the reconstruction reliability within 200 h^{-1} Mpc.

3.2.2. The Reconstruction Algorithm

There are various methods to correct for redshift space distortions which can be divided in two general categories. The first category contains the so called iterative methods derived from that proposed by Strauss & Davis (1988) and used, among the others, by Yahil et al.(1991) and Hudson (1993a). Here the idea is to start from the observed redshift space cluster distribution and attempt to recover the cluster true positions by iteratively computing their peculiar velocities according to eq.(9), assuming therefore linear theory and linear biassing. These methods also require that the mass fluctuations responsible for the peculiar motions are within the volume considered. The second and more recent one contains the direct methods by which the true density field is obtained from the redshift space one by means of some inversion technique that relies on a self–consistent formulation of the linear equation in redshift space. The Nusser & Davis (1994) technique is an example as well as the recently proposed Fisher et al. (1995) method which also minimizes the shot noise error by Wiener filtering.

In this work we use an iterative scheme based on the former methods, to which we refer as *Linear Iterative Reconstruction Algorithm, [LIRM]* and the steps of which are the following:

1. All the clusters are initially placed at their observed distance, $r_z^{(0)} = cz$, with no peculiar velocity and with an arbitrary value for the input β_c parameter. The index $^{(0)}$ refers to the zeroth iteration.

2. The weighting function $w(\mathbf{r}_i)$ is computed and its value is kept constant in the subsequent iterations (i.e. the selection function is not upgraded). This speeds up the algorithm while it also does not lead to appreciable errors, since $P(z) \approx 1$ within 20000 km/sec.

3. The average density n_c within the sampled volume is computed and its value is updated.

4. The window function $W(|\mathbf{r}_i^{(k)} - \mathbf{r}^{(k)}|)$ is computed for each object.

5. The peculiar velocity of the i-th cluster $\mathbf{u}^{(k)}(\mathbf{r}_i)$ is computed according to eq.(12) taking into account both, the clusters within R_{max} and those that during the iterations were placed beyond the volume limits (we will refer to these as 'passive' objects).

6. Radial positions of 'active' clusters are updated. Their new positions are given by

$$r^{(k+1)} = cz - \left[\mathbf{u}(\mathbf{r})^{(k)} - \mathbf{u}(0)^{(k)}\right] \cdot \frac{\mathbf{r}^{(k)}}{|\mathbf{r}^{(k)}|}. \tag{14}$$

   Positions of 'passive' objects are not updated.

7. For each real active cluster we compute the difference of its position between the last two iterations. If the difference is larger than 0.5% r, then we jump back to step (iii). The convergence is typically reached within 10 iterations.

Note that from now on distances are in km/sec units with which we avoid problems related to the definition of distance and to the uncertainties on the Hubble constant.

Since the smoothing scheme treats clusters as spheres of radius R_{sm}, clusters in the spherical shell $|\mathbf{r} - R_{max}| < R_{sm}$ need to be weighted properly by computing how much of the sphere lies within R_{max}. But since we will estimate the dipole and the cluster velocity field only within 20000 km/sec and since we regard the cluster distribution beyond this radius as an improvement over a simple homogeneous distribution, we do not need to implement this correction.

Our iterative reconstruction algorithm can fail to recover the true 3D object position within high cluster density regions ('triple value regions') (cf. Yahil et al. 1991; Hudson 1993a). In our case, however, the objects are so sparsely distributed (which is the reason why the smoothing scale used is relatively large) that this problem is negligible. Obviously, the sparseness of the clusters introduces different problems, as we will discuss below.

3.3. Testing the reconstruction reliability and the stability of our results

To test the *intrinsic* reliability of the whole reconstruction procedure and to optimize its performance we considered a catalogue of mock clusters extracted from a simulation performed by Borgani, Coles & Moscardini (1994) in which the present time cluster positions were determined by the Zel'dovich approximation in a standard CDM model Universe. The mock clusters were identified as peaks above a density threshold which was chosen so that their space density matches that of the observed clusters ($\sim 2 \times 10^{-5} h^3$ Mpc^{-3}). We considered a spherical volume centered around a LG–like observer (see Borgani et al. 1994). Each cluster peculiar velocity was determined according to linear theory after having computed the gravitational acceleration generated by all the clusters within the sampled volume. This ideal cluster distribution was then degraded by Montecarlo rejecting

clusters according to the probability distributions $P(z)$ and $P(b)$ and by devoiding the ZoA. Finally, an artificial Gaussian distributed noise was added to the cluster velocity to mimic experimental errors in their measured redshift. According to observational indications we used a variance of 200 km/sec (Strauss, Cen & Ostriker 1994).

Finally, we applied the *RTCM* together with the *LIRM* to recover the original object distribution and velocities with 10 independent runs to asses the stability of the reconstruction algorithm. Three different indicators were used to assess the *intrinsic* reliability of the reconstruction procedure:

- The difference between reconstructed and true peculiar acceleration acting on the observer.
- The volume averaged discrepancy between the true and the reconstructed position: $\langle \epsilon_i \rangle = \langle |\mathbf{r}_{\mathrm{true,i}} - \mathbf{r}_{\mathrm{rec,i}}| / |\mathbf{r}_{\mathrm{true,i}}| \rangle$
- The spatial cluster–cluster correlation function.

The reconstructed peculiar acceleration vector is very close to the original one. The per cent discrepancy between the amplitudes of the true and the reconstructed peculiar velocities, based on the 10 different reconstructions, was $3 \pm 6\%$. The two vectors were misaligned by $2° \pm 5°$. In Figure 2 we present the distribution of the ϵ_i values which peaks at $\lesssim 1\%$ and has a mean value of $\langle \epsilon_i \rangle \simeq 1.6\%$ (it is skewed towards large errors); while the probability of having $\epsilon_i > 3\%$ is quite low. We found, as expected, that ϵ_i depends on the initial displacement of the i–th cluster with respect to its true position $|\mathbf{r}_{true,i} - \mathbf{r}^{(0)}|$. The reliability of the method greatly improves if clusters are initially placed close to their real positions, which would be possible if reliable redshift independent distance measurements were available for some nearby clusters. Finally, the spatial two point correlation function of the reconstructed cluster distribution turns out to be indistinguishable from the true one.

We stress that these tests are aimed at assessing the *intrinsic* reliability of the reconstruction method; cluster velocities are computed according to linear theory and no allowance for contribution from external gravitational fields is made (a set-up that needs not be true in the real Universe). To get an estimate of the actual uncertainties in the whole procedure we need to account for several other effects, which will be quantified in Section 5.

The *intrinsic* stability of the method has been assessed by computing the variance of the recovered cluster positions after the 10 reconstructions which turned out to be typically ≤ 150 km/sec, being larger near the ZoA and within high density regions and smaller at high galactic latitudes. The stability of the method when applied to the real Abell/ACO catalogue will be quantified in section 4.2.

3.4. Smoothed cluster density maps in z- and 3D–space

In Figure 3a and b we plot in supergalactic Cartesian coordinates the reconstructed whole-sky smoothed density field for a slice of 8000 km/sec wide, centered on the supergalactic plane, in z-space and in 3D space, respectively. Note that the same Gaussian smoothing is used as in figures 1b and 1d and units are km/sec. As also outlined by Scaramella (1994) who derived and discussed similar maps but only in redshift space, the sparseness of the cluster distribution and the heavy smoothing could miss some features of the cosmic density field. Nevertheless, our reconstruction technique should reveal the main large–scale features of the 3D cosmic density field.

From these plots it is evident that eliminating the distortions due to peculiar velocities suppresses significantly the amplitude of the density peaks in 3D with respect to that in the z-space. This effect is particularly evident in the Virgo-Hydra-Centaurus (or else Great Attractor) region [centered at (X,Y) = (-3000,2000)], in the Leo region [centered at (X,Y) = (1000,9000)] and around the Ursa-Major supercluster [centered at (X,Y)=(10000,18000)]. Interestingly, in the Perseus-Pegasus region [centered at (X,Y)=(6000,0)] the opposite is true, ie., the 3D density amplitude is slightly higher than in the z-space case. This could be easily understood if there exists a coherent gradient of negative peculiar velocities, increasing in amplitude towards the near side of this structure (towards smaller X's, ie., towards the LG).

Also, the shape of the density peaks, in the 3D case, appears to be slightly elongated along the line of sight. This effect, which is mostly prominent in the Great Attractor and in the Shapley concentration [centered at (X,Y)=(-8000,8000)], arises from the fact that in the linear regime the infall peculiar velocities within high density regions are coherent and tend to twist the isodensity contours along the line of sight.

In figure 4 we present the 3D cluster density field for the four slices, each of 8000 km/sec width, above and below the supergalactic plane. Panel (*a*) and (*b*) correspond to the $4000 < Z < 12000$ km/sec and $12000 < Z < 20000$ km/sec slices respectively, while panel (*c*) and (*d*) represent the corresponding slices but for negative Z's. Our intention is not to present a detailed analysis of the structures evident in our contour plots (for such a task see Tully 1987 and Tully et al. 1992). However, we would like to emphasize the fact that, most structures found in the supergalactic plane extend not only to the first 8000 km/sec wide slice, above or below the supergalactic plane, but also to the second such slice. For example the overdensity corresponding to the Shapley concentration extends to both negative Z slices. Also the Great Attractor region is connected to the Lepus region [centered at (X,Y)=(-2000,0) in panel *c*] which seems to extend even further to the next slice (panel *d*) while a similar behaviour is found also for Perseus-Pegasus region. From panels (*a*) and (*b*) we see that the same is true for the Ursa Major supercluster, the Grus-Indus region [centered at (X,Y)=(-14000,-16000) in the supergalactic plane slice], the Leo region which seems to be connected with Hercules [centered at (X,Y)=(0,7000) in the (*a*) and (*b*) slices] as well as the Pegasus-Pisces region [centered at (X,Y)=(15000,-13000)] which is evident in the supergalactic plane and the two

positive Z slices.

4. The Abell/ACO Cluster Dipole

The dipole vector, for an observer placed at the center of the coordinate system, is defined as

$$\mathbf{D} = \frac{3}{4\pi} \int \rho_c(\mathbf{r}) \frac{\mathbf{r}}{|\mathbf{r}|^3} d\mathbf{r}, \tag{15}$$

which, in linear theory is related to the peculiar velocity (eq. 12) by $\mathbf{u} = \beta_c H_o \mathbf{D}/3\langle\rho_c\rangle$. For our discrete cluster density field, smoothed with a top hat window, the dipole becomes:

$$\mathbf{D} = \frac{3M_C}{4\pi} \sum_i \left(\frac{M_i}{M_C}\right) w(r_i) W(r_i) \frac{\mathbf{r}_i}{r_i^3} \tag{16}$$

while the monopole of the smoothed field is defined as:

$$M = \frac{M_C}{4\pi} \sum_i \left(\frac{M_i}{M_C}\right) w(r_i) W(r_i) \frac{1}{r_i^2} \tag{17}$$

Computing the dipole and the monopole separately is important for assessing the effective convergence of the peculiar velocity vector since a necessary condition for final convergence is that while the dipole converges, the cumulative monopole continues to grow linearly with distance. This condition, however, is not sufficient to guarantee the final dipole convergence, which could still increase after having reached a *plateau* (cf. Plionis, Coles & Catelan 1993).

One of the major scopes of this work is to compare the cluster dipole as measured in z-space with the reconstructed one in 3D–space. A simple eye inspection of figures 3 a,b revealed that the peaks of the true density field have larger amplitudes when observed in redshift space. However, to see how these distortions affect the estimate of the cluster dipole require a quantitative discussion. From a theoretical point of view the problem has already been addressed by Kaiser (1987). He showed that gravitationally driven peculiar velocities can have a large effect on the peculiar acceleration vector of an object. If D_r is the amplitude of the true dipole and D_z is the z-space dipole, then the relationship between D_r and D_z depends both on the selection function ϕ and on the on the power spectrum considered. If one considers each power mode separately then, in the limit $kR_{max} \gg 1$ (R_{max} is the depth of the survey and k is the wavenumber), Kaiser has shown that

$$\frac{D_z - D_r}{D_r} = \frac{1}{3}\,\beta_c\,[1 + E(k)]\,, \tag{18}$$

where

$$E(k) \simeq \log[(kR_{max})^2 \phi(R_{max})/\phi(k^{-1})]\,. \tag{19}$$

Clearly the sign of $E(k)$ depends on the selection function and on the sample's depth. Although a precise $E(k)$ evaluation requires an accurate determination of the selection function, we are confident

that in our case $\phi(R_{max}) \simeq 1$ which then implies $E(k) > 0$. The final value of $D_z - D_r$ can be obtained in the linear regime by combining each mode separately (for large k the nonlinear evolution couple the different modes, and this approximation does not hold). Obviously to properly combine the different modes requires the knowledge of the density fluctuation power spectrum. However, unless one considers cosmological models with very large power on small scales, which are in conflict with current observations, we expect that for our cluster sample $D_z - D_r > 0$.

4.1. Possible Systematic Effects

The reconstructed cluster distribution could depend on a number of free parameters that are only partially determined by observational constraints and theoretical requirements. We systematically explored the influence of the parameter choice by allowing each free parameter to vary within an experimentally plausible range. In practice the reconstructed cluster dipole, and therefore the predicted LG peculiar velocity, can be regarded as a function of many variables (the free parameters) that are listed in table 1. Boldface quantities refer to what we call the *standard case*, defined by the following choice of parameters: $(\alpha, \alpha) = (0.3, 0.2)$, $R_{sm} = 20\ h^{-1}$ Mpc, $q_o = 0.5$, $\beta_c = 0.25$, direct homogenization scheme (eq.5) with the 200 h^{-1} Mpc sphere being divided into 10 equal volume shells. For each of the 48 possible combinations of the free parameters, to which we refer to as "models", we performed 10 independent reconstructions and we computed the corresponding 3D dipole. To explore the influence of each variable on the predicted LG dipole separately we adopted the following procedure:

- The parameter of interest is selected and models are divided according to the value chosen for that parameter (e.g. $q_o = 0.2$ or 0.5). Models having the same parameter values are grouped in the same category.
- The average dipole at 170 h^{-1} Mpc is computed for all the models in the same category and the same procedure is repeated for all different categories.
- The different average dipoles are compared. The differences in amplitude and the misalignment angles between different average dipoles are listed in table 2.

It is evident from table 2 that the only appreciable systematic effect comes from the choice of the β_c parameter, and not from either the galactic absorption coefficients, the smoothing radius or the Abell-ACO homogenization procedure. To further appreciate the influence of the β_c parameter on the reconstruction process we have to disentangle two different effects: the role of the deceleration parameter, q_o, that enters through eq.(1) in defining the outer limit of the sample, and that of the β_c factor, whose arbitrary initial value has to be specified for the *LIRM* to be applied. The first effect turned out to be much smaller than the second one.

The effect of varying the β_c parameter in the *LIRM* was explored by performing the reconstruction with the same q_o value but using two different β_c values (0.25 and 0.114). Although these values are different by a factor ~ 2, the asymptotic amplitudes of the reconstructed dipole are very similar, differing only by 8%, being smaller for the standard $\beta_c = 0.25$ case, while the direction does not change appreciably.

It is interesting to compare this result to that obtained by Strauss et al. (1992, [hereafter SYDHF92]). The asymptotic amplitude of their IRAS galaxy dipole, on scales larger than $\sim 100\ h^{-1}$ Mpc, strongly depends on the input β_c value. The reason for this behaviour was ascribed to redshift space distortions, to which they refer as the 'Kaiser effect', that in their case is mainly due to the LG motion with respect to the distribution of distant galaxies. In this simple situation the problem is similar to that of a 'rocket–born' observer who resides in a uniform Universe at rest with respect to the CMB on large-scales and whose peculiar acceleration originates locally (Kaiser & Lahav 1988). In this idealized case the redshift space distortions appreciably affect the measured peculiar acceleration only if the selection function ϕ falls below one, well within the sample's depth. This is the case for the IRAS galaxy sample studied by SYDHF92, where $\phi \ll 1$ well within 100 h^{-1} Mpc. For our sample, however, $P(z)$ is close to unity within 200 h^{-1} Mpc so that the 'Kaiser Effect' is much less important, as demonstrated by the stability of our dipole against the variations of β_c; especially at large depths where the sensitivity to the input β_c-parameter would be manifested by variations of the dipole amplitude shape as a function of β_c (cf. Fig.6 of SYDHF92).

4.2. Error Estimate

To obtain a reliable error estimate of the reconstructed dipole we need to account for several different sources of errors. We estimate the *intrinsic* error, σ_i, in the reconstruction algorithm from the 10 independent reconstructions performed for each model explored The *intrinsic* error (which is typically smaller than 150 km/sec) represents therefore a stability measurement of the reconstruction procedure. Other sources of errors, which will be described below, are the observational error σ_o and the 'shot–noise' error σ_{sn}. In what follows we will assume that all these errors are independent so that the total uncertainty σ_T will be simply estimated by adding the errors in quadrature.

4.2.1. Observational error

We define as observational error the uncertainty derived from the different free parameter choice, listed in table 1, whose separate influence on the reconstructed dipole was explored in the previous subsection. The reconstructed dipole can be therefore regarded as a function of the smoothing length, the homogenization scheme and its binning, parameters that we allowed to vary in a plausible range

of values. The galactic absorption set and the β_c factor, instead, are considered fixed by observations to $(0.2, 0.2)$ and to $\beta_c = 0.25$, respectively. We chose $\beta_c = 0.25$ since, as we will see in section 5, this value is closer to that one derived from the comparison with the CMB dipole. We found that varying these parameters does not produce any systematic effect in the dipole determination and thus we can consider them as Gaussian variables and the dipole as a multivariate Gaussian function of the explored parameters. Following this argument we compute σ_0 as the variance of the dipole obtained by averaging over all models having $(\alpha, \alpha) = (0.3, 0.2)$ and $\beta_c = 0.25$ (our standard case). The observational error at 170 h^{-1} Mpc produces an uncertainty of $\sim \pm 65\ \beta_c^{-1}$ km/sec in the dipole amplitude and of $\pm 4°$ and $\pm 2°$ along b and l directions respectively.

4.2.2. Shot-Noise error

The usual shot–noise estimate assumes that luminous objects have been drawn by a Poisson process from the underlying density field. However the reconstruction procedure relies on the hypothesis that clusters of galaxies are *biased* tracers the mass. A more meaningful and self–consistent estimate of the shot noise error has been proposed by SYDHF92 that accounts for two different effects:

- The Poissonian error due to the fact that luminous objects become random tracers of the density field when the selection function falls below unity.
- An uncertainty due to the fact that cluster masses are randomly taken from an underlying mass distribution. In our case we estimated the mass of real clusters from their Abell listed number of galaxies while for synthetic clusters, which constitute $\sim 50\%$ of the whole cluster population, the mass was set equal to the average real cluster mass.

Using our formalism, the SYDHF92 shot noise computed for the $\mathcal{W}_{rel} = 1$ case, reduces to:

$$\sigma_{sn}^2 = \left(\frac{\beta_c}{4\pi n_c}\right)^2 \sum_i^{N_s} \frac{W(r_i)^2}{r_i^4} K\left[\tilde{w}(r_i) - 1\right], \tag{20}$$

where the sum extends only over the N_s synthetic clusters, n_c is the average cluster density defined from eq.(13) and $K = \langle \mu_i^2 \rangle - 1$, with μ_i being the mass of the real clusters in units of average mass. From the real clusters mass variance we have K=0.25. To compute the influence of the shot noise on the amplitude and the direction of the dipole we will assume that each component of the dipole is a Gaussian with zero mean and $\sigma_{sn,x} = \sigma_{sn,y} = \sigma_{sn,z}$. The 1-dimensional shot noise error at 170 h^{-1} Mpc reflects in an $\sim \pm 60\ \beta_c^{-1}$ km/sec amplitude and a $\sim \pm 4°$ directional uncertainty.

4.3. The 3D Cluster Dipole

After reconstructing the cluster distribution with the *RSCM* and the *LIRM*, we computed the cluster dipole both in redshift and real–space. Figure 5a shows the amplitude of the peculiar velocity for the standard model, computed using eq.(12), as a function of distance. Open dots refer to the z-space dipole while filled symbols represent the reconstructed 3D cluster dipole. We also plotted, for reference, the dipole computed without any Abell/ACO homogenizing scheme (i.e. $\mathcal{W}_{rel} = 1$) in z-space (continuous line). Errorbars represent 1 σ total errors.

Our main result is that the asymptotic value of the 3D dipole, D_r, is significantly less than the corresponding z-space one, D_z, as predicted by eq.(18). Removing redshift space distortions erases the artificial redshift space clustering, leading to $(D_r - D_z)/D_z \approx -0.23$ or else $(D_z - D_r)/D_r \approx 0.3$. Although the amplitude of the 3D dipole is significantly less than what previously found in cluster-dipole z-space studies (PV91; SVZ91), the qualitative dipole behaviour is similar in z-space and 3D–space: a "bump" of the velocity amplitude around $50h^{-1}$ Mpc followed by a decrease due to the competing pull of the Great Attractor with the Perseus–Pegasus regions, a secondary increase after a *plateau* and an asymptotic convergence beyond $\sim 170\ h^{-1}$ Mpc once that the Shapley concentration has entered into the sampled volume. The mass distribution beyond 60 h^{-1} Mpc is responsible for $\sim 30\%$ of the total LG peculiar acceleration. As already noticed from the qualitative analysis of the density field maps, the effect of eliminating the apparent z-space clustering is particularly important in local high density regions, such as the GA area, which is clearly responsible for the significant decrease of the $\sim 50\ h^{-1}$ Mpc bump in the 3D cluster dipole case. In Figure 5a we also plot, in arbitrary units, the 3D space monopole term, which grows linearly out to the depths sampled which indicates that the dipole convergence at $\sim 170\ h^{-1}$ Mpc is not an artifact of ill sampling.

Figure 5b displays the cumulative direction of the LG velocity. The starred symbol indicates the CMB dipole apex, while the skeletal symbol represents the CMB direction after correcting the LG for a Virgocentric infall of 200 km/sec. Errorbars represent the 1 σ total errors. The relatively large error ($\sim 10°$) in the dipole direction, along b, is due to the uncertainty related to the amplitude of the Virgocentric infall. The reconstructed 3D dipole points $\sim 10°$ away from the CMB apex when the Virgo infall is taken into account. No significant differences between the 3D and z-space dipole directions was found.

4.3.1. The effect of varying the Mask model

It is interesting to investigate the influence of the Mask model, adopted to reconstruct the whole sky z-space cluster distribution, on the reconstructed dipole.

We explored two variants of the *RSCM*. In the first one we fill independently the northern and southern parts of the ZoA by applying the *[RSCM]* to the northern and southern adjacent galactic strips ($20° \leq |b| \leq 43.16°$) separately. In the second case we identify the ZoA with the equatorial

strip $|b| < 13°$ and then we consider the two adjacent strips defined so that their ***individual*** solid angles are equal to that of the ZoA. The *[RSCM]* is then applied by half counting the number of clusters in the adjacent bins. In both cases there is a small increase of the dipole's amplitude, by $\sim 3\% - 4\%$, and the direction points $\sim 4 \pm 4°$ away from the original one (uncertainties refer to the intrinsic errors). We conclude that no significant dependence was found on the Mask choice, which is to be expected since all of them are based on a cloning scheme.

A more relevant comparison is probably between two conceptually different methods. For example between our *RSCM* and the spherical harmonic reconstruction method (cf. Lahav 1987; Yahil et al 1986; Plionis 1988 and PV91 for use of this method in the cluster dipole context). In Figure 6 we compare our standard *RSCM* z-reconstructed dipole with that derived using the PV91 method for the same sample and the same set of parameters. In the insert we plot the relative velocity fluctuations, defined as $2 \times (v_{RSCM} - v_{SH})/(v_{RSCM} + v_{SH})$. It is evident that both methods give identical results, except in the inner volume ($\lesssim 50\ h^{-1}$ Mpc) where the number of clusters is extremely small and therefore shot noise effects are large. This is quite extraordinary given the completely different methods used.

Finally, we also use an alternative scheme to reconstruct the region beyond 200 h^{-1} Mpc which is based on extending the reconstruction technique used in the inner volume to the external region, coupled with the *RSCM*. We found that the 3D dipole differs from the standard one only beyond 200 h^{-1} Mpc, where the amplitude monotonically increases (by $\sim 8\%$) and the direction systematically drifts towards lower galactic latitudes. As we discussed in section (3.1), using this schemes increases the shot noise errors in a region where the selection function is significantly smaller than 1 and then is probably responsible for the drift in the dipole direction, while it also enhances the 'Kaiser Effect' which causes the observed amplitude increase.

4.3.2. Abell richness dependent effects

As discussed in section 2, our Abell/ACO sample includes also richness class $R = 0$ clusters which although suspect of being incomplete, such effect is not apparent within the volume considered in our analysis. However we have tested, using the above mentioned Spherical Harmonic method, the effect of excluding them from our dipole analysis. Using $R \geq 1$ clusters we reduce our original sample by $\sim 57\%$ but we still find that their dipole has a similar overall shape with that of the $R \geq 0$ case; similar convergence depth ($\sim 170\ h^{-1}$ Mpc) and CMB-alignment ($\delta\theta_{cmb} \lesssim 20°$) while their amplitude difference is $\delta v \sim -15\%$. We are therefore confident that the possible incompleteness of the $R = 0$ sample does not significantly affect the behaviour and asymptotic value of our cluster dipole and it probably becomes important only at distances considerably larger than the apparent cluster dipole convergence depth (see section 2.2 and Postman et al. 1992).

We point out however, that the $R \geq 1$ dipole increases initially in a much smoother fashion than the corresponding $R \geq 0$ one, which is due to the fact that 10 out of the 12 clusters within $\sim 60\ h^{-1}$ Mpc are $R = 0$ clusters and it is these clusters that constitute the large overdensities seen in the *Great Attractor* and Perseus-Pisces regions (see figure 3), and thus responsible for the initial kick of the LG peculiar acceleration.

5. Constraints on the Value of β_c

¿From the measured asymptotic value of the cluster dipole it is possible to constrain the value of β_c. An estimate of this parameter can be obtained by using the fact that the cluster 3D dipole has converged to its final value at $\sim 170\ h^{-1}$ Mpc, in accordance with SVZ91 and PV91. We have, however, to take into account a zero-point offset in the cluster-dipole which originates from the fact that the Abell-like Virgo cluster, due to its proximity and thus low surface brightness, is not included in the Abell/ACO catalogue and therefore its contribution to the cluster dipole has been missed. A possible way to deal with this problem is to merge the cluster dipole with that of some galaxy sample that trace more densely the local mass distribution (Scaramella et al. 1994). With this approach, however, the offset can be evaluated only assuming an *a priori* value of the cluster–galaxy relative bias, whose value is very uncertain (for a complementary approach see Plionis 1995). Instead we adopt a simpler phenomenological correction by identifying the zero point offset with the LG Virgocentric infall, the velocity of which we take to be $V_{inf} \approx 170$ km/sec. We choose this value to be the average of the traditional ~ 260 km/sec value with the lower one of Faber & Burstein (1988) [~ 85 km/sec].

Comparing the cluster dipole amplitude to the LG peculiar velocity (as inferred by the CMB dipole) via eq.(12), we then obtain:

$$\beta_c = 0.21(\pm 0.03)\, f(V_{inf})\,, \qquad f(V_{inf}) \equiv \left[\frac{622 - V_{inf}\cos\delta\vartheta}{622 - 170\cos\delta\vartheta}\right] \tag{21}$$

where the function $f(V_{inf})$ represents the parameterization of V_{inf} and $\delta\vartheta$ is the angle between the Virgo and CMB dipole directions; $\sim 45°$. If we erroneously did not account for the Virgo infall we would obtain $\beta_c \approx 0.26$ and similarly if the Virgocentric infall velocity is underestimated then a lower value of β_c can be obtained (for example if $V_{inf} = 260$ km/sec then $\beta_c \approx 0.18$). The quoted uncertainty in eq.(21) comes from the total dipole scatter, as discussed in section 4, Although this uncertainty is quite wide, our estimate of the value of β_c is still more than $\sim 2\sigma$ larger that previous estimates based on the z-space cluster distribution (PV91, SVZ91, Scaramella et al. 1994). Assuming $\Omega_o = 1$ we obtain a cluster bias parameter with respect to the underline mass distribution of:

$$b_c = 4.8(\pm 0.8).$$

According to the linear biasing prescriptions if b_A and b_B are the biasing factors of objects A and B with respect to the matter with $b_A > b_B$, the following relation holds: $b_{AB} \sim b_A/b_B$, where b_{AB} is

the biasing factor of objects A with respect to objects B. If the biasing factor of Abell/ACO clusters with respect to IRAS galaxies is $b_{cI} \lesssim 4.5$ (cf. Peacock & Dodds 1994; Jing & Valdarnini 1993) we have that the above b_c value is consistent with a bias parameter of IRAS galaxies with respect to the mass of $b_I \gtrsim 1.1^{+0.7}_{-0.3}$.

A final note regarding the possible external contributions to the cluster dipole. Juskiewicz, Vittorio & Wyse (1990) computed the probability distribution of the peculiar velocity of a generic observer, constrained to be moving with a velocity of 620 km/sec with respect to the CMB, as a function of the sampled volume. From this distribution they computed the expectation value for the estimated LG velocity and its variance (their eq. 8a and 8b). The expectation value at 170 h^{-1} Mpc weakly depends on the cosmological model adopted. We explored a number of possible models ranging from the Standard CDM one to the phenomenological model proposed by Branchini et al. (1994) that resembles a tilted CDM with $n = 0.7$ and to the Peacock & Nicholson (1994) spectrum with more power on large scale (similar to a standard CHDM model). In all these cases the expectation value for the LG velocity, at 170 h^{-1} Mpc coincides with the true one. Also the variance slightly depends on the cosmological model, being larger in correspondence to the Peacock & Nicholson (1994) spectrum. We take as the typical cosmic variance the value $\sim 150\ \beta_c^{-1}$ km/sec, which then gives a further uncertainty in β_c of $^{+0.08}_{-0.05}$.

6. Conclusions

In this work we described a self consistent method to reconstruct the 3D distribution and peculiar velocities of galaxy clusters from their observed positions in the redshift space. Our approach is valid within the framework of gravitational instability and relies on the assumption of linear theory and linear biasing. The technique presented aims at recovering, in a statistical sense, the distribution of unobserved clusters and corrects the apparent cluster positions for peculiar velocity driven redshift space distortions. Tests performed using synthetic cluster distributions, obtained from numerical experiments, showed that the intrinsic reliability of this technique allows the true cluster positions to be recovered with an average error of ~ 1.6 %, much better than the best available experimental determination of cluster distances ($\gtrsim 10\%$). However, the actual reconstruction uncertainty is larger since we adopted a phenomenological method, to reconstruct the whole sky z-space distribution of clusters, characterized by several parameters with associated observational errors. As necessary in any phenomenological approach, we tested the stability of the final results on the various experimental parameters and found them to be surprisingly robust.

The main result of this first paper is that redshift space distortions cause an artificial increase of the cluster dipole amplitude by $\sim 23\%$, while they do not affect appreciably the dipole direction which points $\sim 10°$ away from the CMB apex. The cumulative 3D dipole qualitative matches the

behaviour of the z-space one: there is a bump at $\sim 50\ h^{-1}$ Mpc and, after a *plateau*, it rises by $\sim 30\%$ and stabilizes beyond $170\ h^{-1}$ Mpc where it reaches a real, although not necessary final, convergence. The reduction of the 3D dipole amplitude with respect to that of the z-space one arises mainly from the removal of the strong apparent clustering in the Great Attractor and Shapley regions and its enhancement in the Perseus-Pegasus region, as can be clearly seen in the smoothed density maps of Figure 3a,b. These results are robust in the sense that a search for the presence of systematic biases gave negative results. In practice we found that the freedom of modelling the galactic absorption, the radial selection function, the ZoA filling scheme, the homogenization and the smoothing procedures cause systematic errors much smaller than the intrinsic error in the reconstruction procedure. Interestingly, since the selection function of our cluster sample is ~ 1 up to $\sim 190\ h^{-1}$ Mpc, our 3D dipole determination is only marginally affected by the 'Kaiser effect' which has been found to be a serious problem in the 3D galaxy dipole estimations.

From the asymptotic dipole amplitude we have estimated $\beta_c = 0.21(\pm 0.03)$. This value is larger than previously found based on the analysis of the z-space cluster distribution, the reason being that we have accounted for redshift space distortions. The intrinsic cosmological variance, however, reflects in a larger uncertainty whose magnitude depends on the unknown cosmological background. In the conservative and widely accepted hypothesis that the cosmic density field is characterized by a large correlation length we estimate the cosmic variance to provide a further uncertainty of $\delta\beta_c \sim 0.07$ and therefore we cannot set stringent limits on the value of β_c. Better constraints may be obtained from the comparison of the reconstructed cluster peculiar velocities with those determined observationally that we will present in a forthcoming paper.

Acknowledgements

We would like to thank Prof. Dennis W. Sciama for suggesting to us a problem out of which the idea for this work was born. We also thank Dr. Stefano Borgani for giving us access to his Zel'dovich cluster simulations. MP acknowledges receipt of an EEC *Human Capital and Mobility Fellowship.*

REFERENCES

Abell G.O., 1958, ApJ, 3, 211

Abell G.O., Corwin H.G., Olowin R.P., 1989, ApJS, 70, 1

Bahcall N.A., Soneira R.M., 1983, ApJ, 270, 20

Bahcall N.A., Gramman, M. & Cen, R., 1994, ApJ, 436, 23

Batuski D.J., Bahcall N.A., Olowin R.P., Burns J.O., 1989, ApJ, 341, 599

Borgani, S., Coles, P. & Moscardini, L., 1994, MNRAS, 271, 223

Branchini E., Guzzo L., Valdarnini R., 1994, ApJ, 424, L5

Branchini E. & Plionis M., 1995, XVth Moriond proceedings on Clustering in the Universe, in press Institute of Physics Publishing Bristol and Philadelphia.

Croft R.A.C., Efstathiou G., 1994, Large Scale Structure in the Universe, ed Mücket J. P., et al., World Scientific, In press

Courteau S., Faber S.M., Dressler A., Willick J.A., 1993, ApJ, 412, L51

Dekel A., 1994, ARA&A, 32, 99

Dressler A., Faber S.M., 1990, ApJ, 354, 13

Faber S.M. & Burstein D., 1988, in Large Scale Motions in the Universe: A Vatican Study Week, p. 115, eds Rubin V.C. & Coyne G., Princeton Univ. Press, Princeton.

Feldman H.A., Watkins R., 1994, 430, L17

Fisher K.B., Lahav O., Hoffman Y., Lynden–Bell D & Zaroubi S. MNRAS 1995 272 885

Han M., Mould J., 1990, ApJ, 360, 448

Huchra, J.P., Henry, J.P., Postman, M. & Geller, M.J. 1990, ApJ, 365, 66

Hudson M.J., 1993a, MNRAS, 265, 43

Hudson M.J., 1993b, MNRAS, 265, 72

Hudson M.J., 1994, MNRAS, 266, 475

Jaffe A.H., Kaiser N., 1994, CITA Preprint

Jing Y.P., Plionis M., Valdarnini R., 1992, ApJ, 389, 499

Jing Y.P. & Valdarnini R., 1993, ApJ, 406, 6

Juskiewicz R., Vittorio N., Wyse R.F.G., 1990, ApJ, 349, 408

Kaiser N., 1984, ApJ, 284, L9

Kaiser N., 1987, MNRAS, 227, 1

Kaiser N., Lahav O., 1988, Large Scale Motions in the Universe: A Vatican Study Week, p. 339, eds Rubin V.C. & Coyne G., Princeton Univ. Press, Princeton.

Kogut A., Lineweaver C., Smoot G.F., Bennet C.L., Banday A., Bogges N.W., Cheng E.S., De Amici G., Fixsen D.J., Hinshaw G., Jackson P.D., Janssen H., Keegstra P., Lowenstein K., Lubin P., Mather J.C., Tenorio L., Weiss R., Wilkinson D.T., Wright E.L., 1993, ApJ, 419, 1

Kolokotronis, V., Plionis, M., Coles, P., Borgani, S. & Moscardini, L., 1995, MNRAS, submitted

Lahav O., 1987, MNRAS, 225, 213

Lahav O., Rowan-Robinson, M. & Lynden-Bell, D., 1988, MNRAS, 234, 677

Lahav O., Edge A.C., Fabian A.C., Putnet A., 1989, MNRAS, 238, 881

Lauer T.R., Postman M., 1994, ApJ, 425, 418

Lubin P., Villela., 1986, Ann NY Acad. Sci., 470, 383

Lynden-Bell D., Lahav, O. & Burstein, D., 1989, MNRAS, 241, 325

Lynden–Bell D., Faber S.M., Burstein D., Davies R.L., Dressler A., Terlevich R.J., Wegner G., 1988, ApJ, 326, 19

Mathewson D.S., Ford V.L., 1994, ApJ, 434, L39

Meiksin A., Davis M., 1986, AJ, 91, 191

Miyaji T., Boldt E., 1990, ApJ, 353, L3

Mould J.R., Staveley–Smith L., Schommer R.A., Bothun G.D., Hall O.J., Han M., Huchra J.P., Roth J., Walsh W., Wright A.E., 1991, ApJ, 383, 476

Nusser A. & Davis M. ApJ 421, L1

Peacock J.A., Nicholson D., 1991, MNRAS, 253, 307

Peacock J.A. & Dodds, S.J., 1994, MNRAS, 267, 1020

Peacock J.A. & West M., 1992, MNRAS, 259, 494

Peebles P.J.E., 1980, The Large Scale Structure of the Universe, Princeton University Press, Princeton

Plionis M., 1995, XVth Moriond proceedings on Clustering in the Universe, in press

Plionis M., 1988, MNRAS, 234, 401

Plionis M., Valdarnini R., 1991, MNRAS, 249, 46 (PV91)

Plionis M., Valdarnini R., Jing Y.P., 1992, ApJ, 398, 12

Plionis M., Coles P., Catelan P., 1993, MNRAS, 262, 465

Postman M., Huchra, J.P., Geller, M.J., 1992, ApJ, 384, 407

Postman M., Spergel D.N., Satin B., Juskiewicz R., 1989, ApJ, 346, 588

Rowan–Robinson M., Lawrence A., Saunders W., Crawford J., Ellis R., Frenk C.S., Parry I., Xiaoiang X., Allingtin–Smith, J., Efstathiou G. Kaiser N., 1990, MNRAS, 247, 1

Rubin V.C., Thonnard N., Ford W.K.Jr., Roberts S.M., 1976, AJ, 81, 719

Scaramella R., Zamorani G., Vettolani G., Chincarini G., 1990, AJ, 101, 342

Scaramella R., Vettolani G., Zamorani G., 1991, ApJ, 376, L1 (SVZ91)

Scaramella R., Vettolani G., Zamorani G., 1994, ApJ, 422, 1 (SVZ94)

Scaramella R., 1995, proceedings of XVth Moriond Astrophysics Meeting, in press

Strauss M.A., Davis, M., 1988, Large Scale Motions in the Universe: A Vatican Study Week, p. 255, eds Rubin V.C. & Coyne G., Princeton Univ. Press, Princeton.

Strauss M.A. & Willick J.A., 1995, Phys.Rep., in press

Strauss M.A., Yahil A., Davis M., Huchra J.P., Fisher K., 1992, ApJ, 397, 395 (SYDHF92)

Strauss M., Cen R., Ostriker J.P., 1994, Cosmic Velocity Fields, p. 437, eds Bouchet F.R. & Lachieze–Rey M., Editions Frontieres.

Tini-Brunozzi S., Borgani, S., Plionis, M., Moscardini, L., Coles, P., 1995, MNRAS, in press.

Tully R.B., 1987, ApJ, 323, 1

Tully R.B., Scaramella, R., Vettolani, G. & Zamorani, G., 1992, ApJ, 388, 9

Villumsen J.V., Strauss M.A., 1987, ApJ, 322, 37

Vittorio N., Juskiewicz, R., 1987, Nearly Normal Galaxies, p.451, ed Faber S.M., Springer–Verlag

Willick J.A., 1990, ApJ, 351, L45

Yahil A., Sandage A., Tamman G.A., 1980, ApJ, 242, 448

Yahil A., Walker D., Rowan–Robinson M., 1986, ApJ, 301, L1

Yahil A., Strauss M.A., Davis M., Huchra J.P., 1991, ApJ, 372, 380

This manuscript was prepared with the AAS LaTeX macros v3.0.

Table 1: Experimental Parameters. Boldface quantities represent the 'Standard Model' set.

Galactic absorption coefficients[1]	**(0.2,0.3)**		(0.2,0.2)
Deceleration parameter q_o	0.2		**0.5**
Smoothing length Mpc h^{-1}[2]	10	**20**	30
$W_{rel}(r)$ binning[3]	**10**		15
Abell-ACO homogenization scheme[4]	**Direct**		Inverse

[1] Strength of the galactic absorption (eq.2).

[2] Smoothing radius of the top hat sphere.

[3] Number of radial bins dividing the 200 Mpc h^{-1} sphere.

[4] Homogenization scheme as described in section 2.2.

Table 2: Cluster dipole variations as a function of different parameters.

Parameters	Δu	Δl	Δb
(0.2,0.3) vs. (0.2,0.2)	$-1 \pm 10\%$	$+3 \pm 5°$	$-2 \pm 4°$
$\beta_c = 0.25$ vs. $\beta_c = 0.114$	$-8 \pm 12\%$	$0 \pm 5°$	$-1 \pm 4°$
R_{sm} = 20 Mpc vs. R_{sm} =10 Mpc	$-3 \pm 11\%$	$0 \pm 4°$	$+3 \pm 3°$
R_{sm} = 20 Mpc vs. R_{sm} =30 Mpc	$-2 \pm 11\%$	$+1 \pm 4°$	$+1 \pm 4°$
bin = 10 vs. bin=15	$-4 \pm 11\%$	$+1 \pm 4°$	$0 \pm 4°$
Direct vs. Inverse	$+4 \pm 11\%$	$+1 \pm 4°$	$0 \pm 4°$

First column displays the parameters defining the two compared categories. Column 2 shows the % difference of the dipole amplitude at 170 h^{-1} Mpc together with the relative standard deviation. Columns 3 and 4 contain the average misalignment and its standard deviation at 170 h^{-1} Mpc along l and b, respectively.

Figure Captions

Figure 1:

(a) and (c): The projected whole-sky z-space cluster distribution in Cartesian supergalactic coordinates. Filled symbols represent real Abell/ACO clusters while open symbols the synthetic objects. Short dashed lines delineate the $|b| \leq 20°$ region. (a) X_{sup}-Y_{sup} projection and (c) X_{sup}-Z_{sup} projection.

(b) and (d): The projected smoothed whole-sky z-space cluster density field (of panels (a) and (c)). A 2–D Gaussian kernel was used with R_{sm} = 2000 km/sec. (b) X_{sup}-Y_{sup} projection and (d) X_{sup}-Z_{sup} projection.

Figure 2: The distribution of relative percentage differences, ϵ_i, between the true and reconstructed positions of simulated clusters (see text for details) which were used to assess the reliability of our reconstruction method.

Figure 3: The projection onto the supergalactic plane of the smoothed cluster density field with $-4000 < Z_{sup} < 4000$ km/sec. (a) z-space (b) reconstructed 3D-space. Same smoothing procedure and same units used as in figure 2.

Figure 4: X_{sup}-Y_{sup} projections of the smoothed 3D-space cluster density field for 4 slices in Z_{sup}. Units used are km/sec. (a) $4000 < Z_{sup} < 12000$ km/sec. (b) $12000 < Z_{sup} < 20000$ km/sec. (c) $-12000 < Z_{sup} < -4000$ km/sec. (d) $-20000 < Z_{sup} < -12000$ km/sec.

Figure 5: Cluster dipole.

(a) Dipole amplitude as a function of distance with open symbols representing the reconstructed whole-sky z-space dipole and filled ones the reconstructed 3D dipole. The continuous thin line refers to the z-space dipole without any Abell/ACO homogenizing scheme (i.e. $\mathcal{W}_{rel} = 1$). In arbitrary units, we plot also the 3D-space monopole (small filled squares).

(b) Dipole misalignment angle. The starred symbol indicates the CMB dipole apex, while the skeletal symbol represents the same but after correcting for a Virgocentric infall component of the LG motion, with an amplitude of 200 km/sec.

Errorbars are 1 σ total uncertainty (see text for details).

Figure 6: Comparison of the z-space dipole derived by using our standard *RSCM* method to reconstruct the whole-sky cluster distribution and that derived using the spherical harmonic method (cf. PV91) for the same sample and the same set of parameters. In the insert we plot the relative velocity fluctuations between the two determinations.

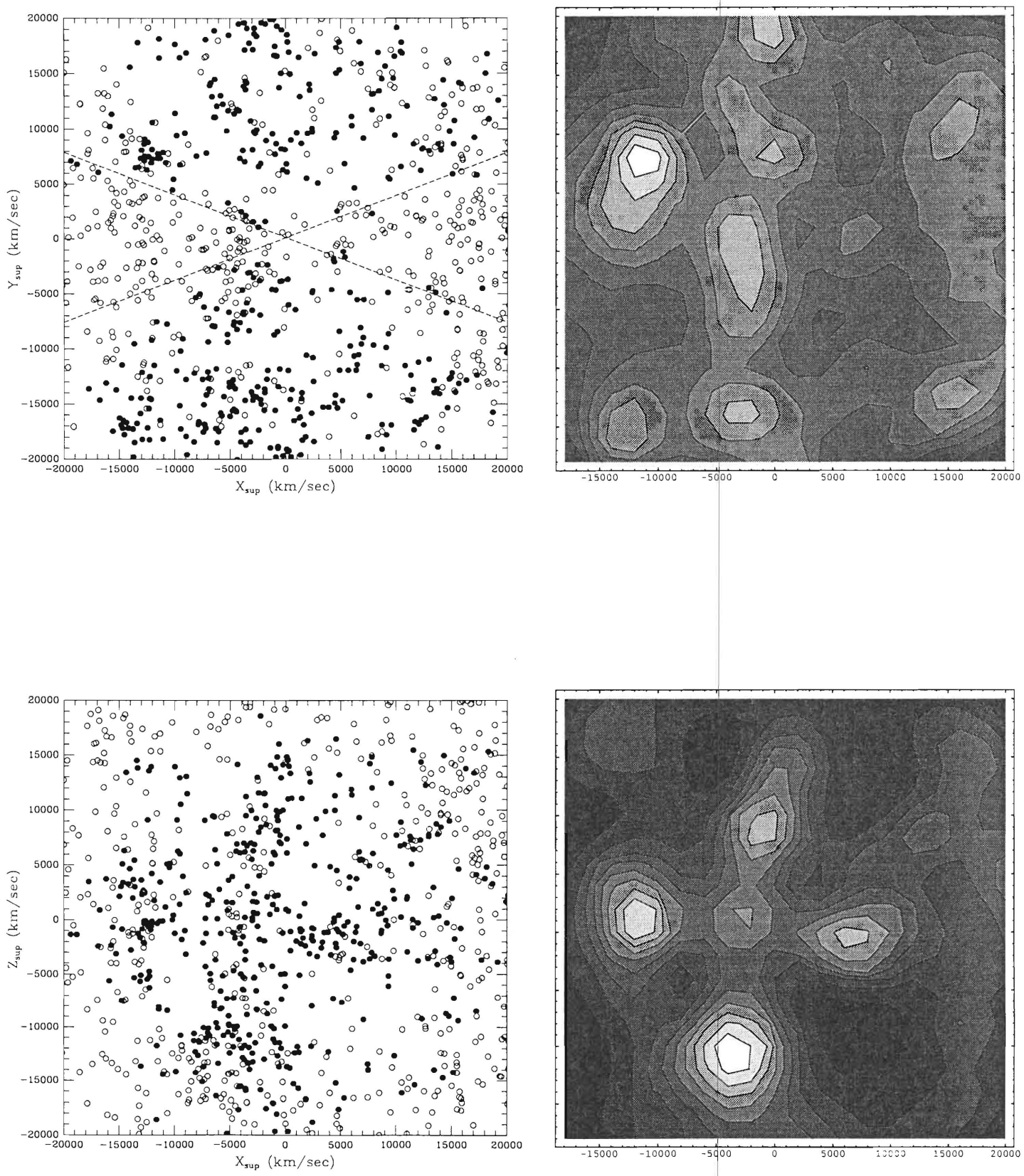
20000
15000
10000
5000
0
-5000
-10000
-15000
-20000
Y_{sup} (km/sec)
X_{sup} (km/sec)
Z_{sup} (km/sec)
-20000 -15000 -10000 -5000 0 5000 10000 15000 20000
-15000 -10000 -5000 0 5000 10000 15000 20000

fig 1

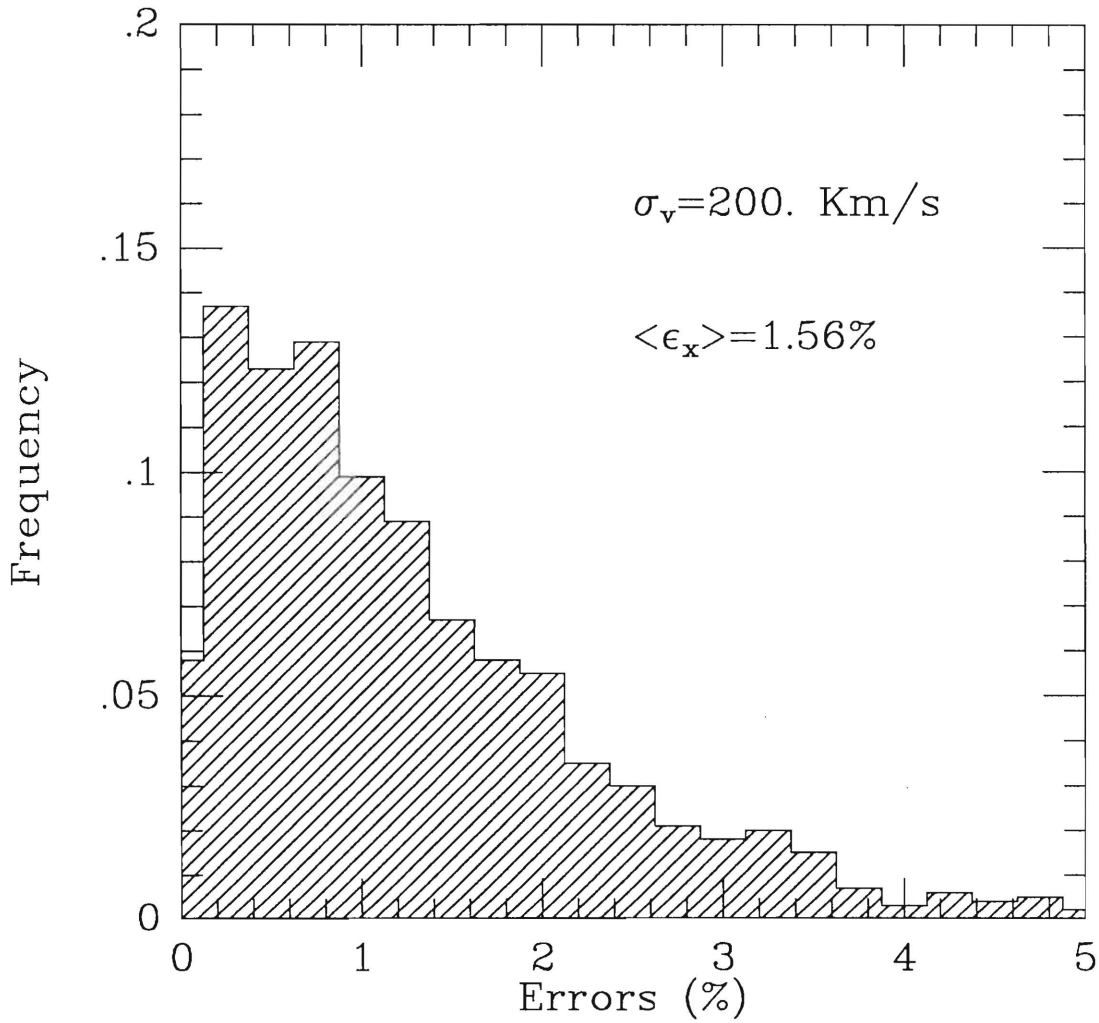
.2
.15
.1
.05
0
Frequency
σ_v=200. Km/s
$<\epsilon_x>$=1.56%
0
1
2
3
4
5
Errors (%)

fig 2

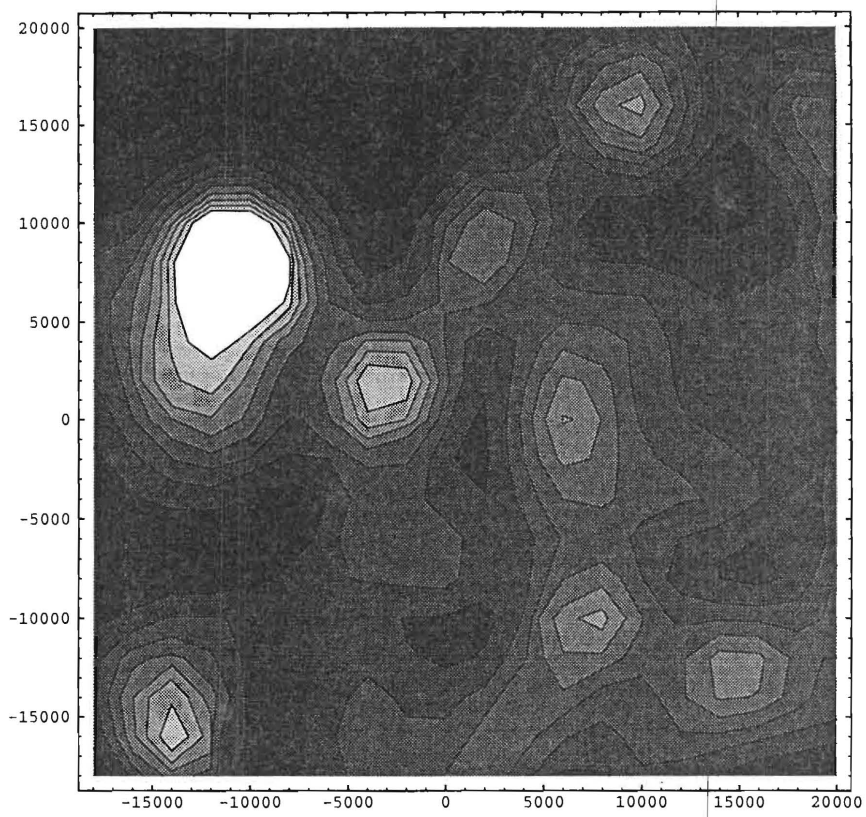
20000
15000
10000
5000
0
-5000
-10000
-15000
-15000
-10000
-5000
0
5000
10000
15000
20000

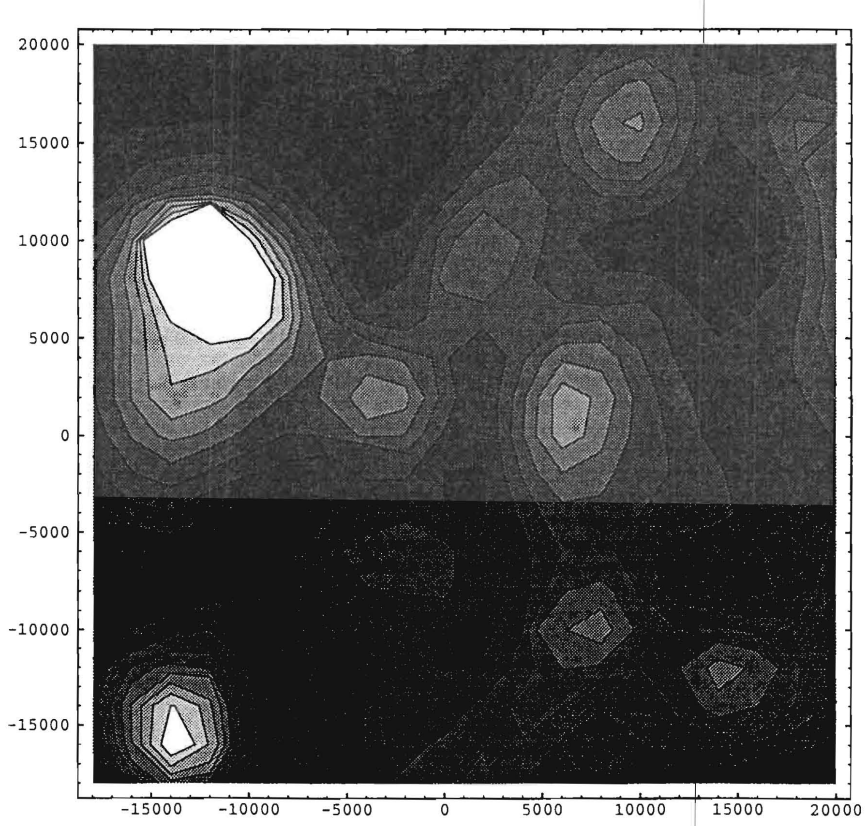
20000
15000
10000
5000
0
-5000
-10000
-15000
-15000
-10000
-5000
0
5000
10000
15000
20000

fig 3

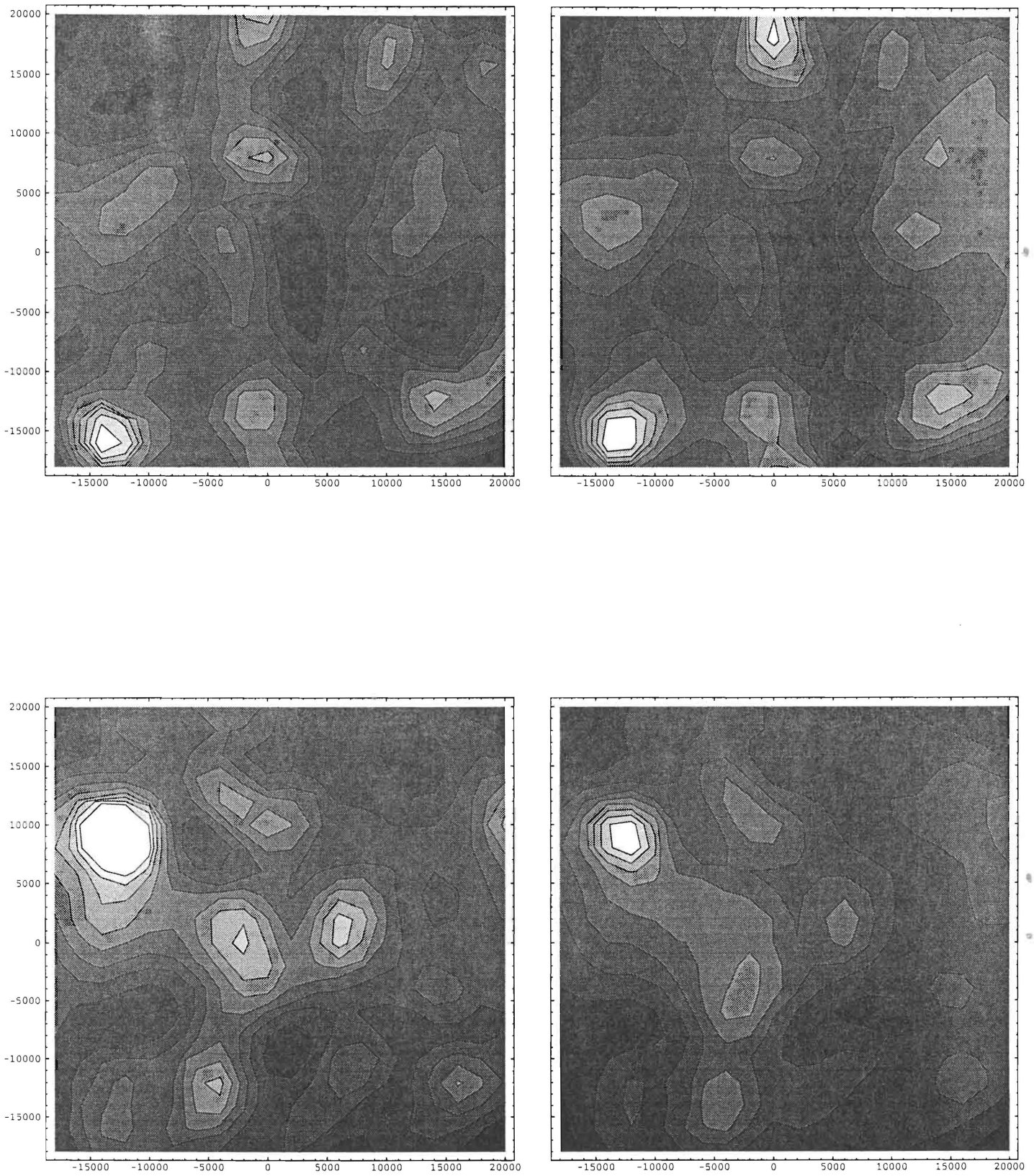
20000
15000
10000
5000
0
-5000
-10000
-15000
-15000 -10000 -5000 0 5000 10000 15000 20000

fig 4

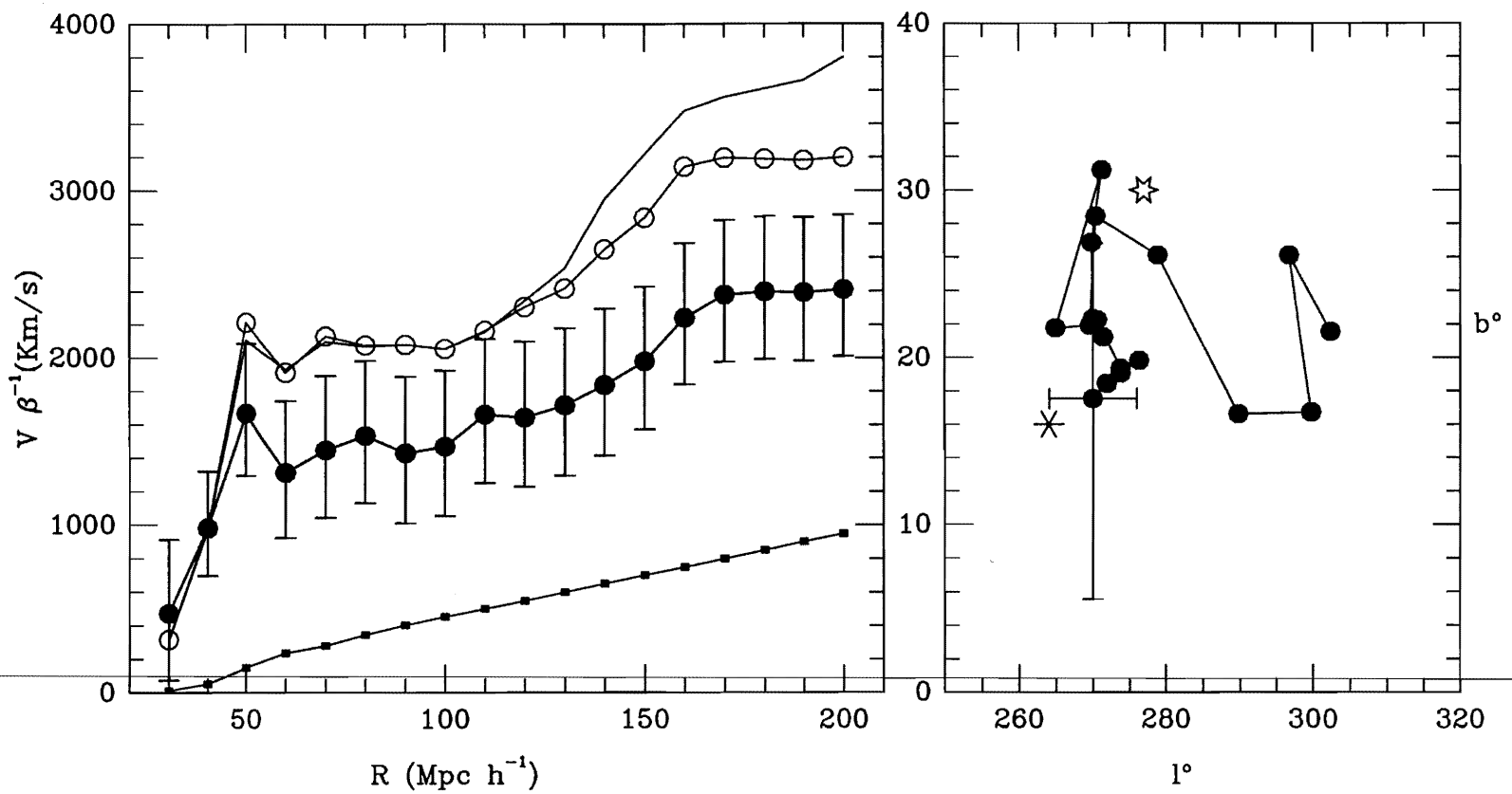
4000
3000
2000
1000
0
V β^{-1}(Km/s)
50
100
150
200
R (Mpc h^{-1})
40
30
20
10
0
260
280
300
320
l°
b°

fig 5

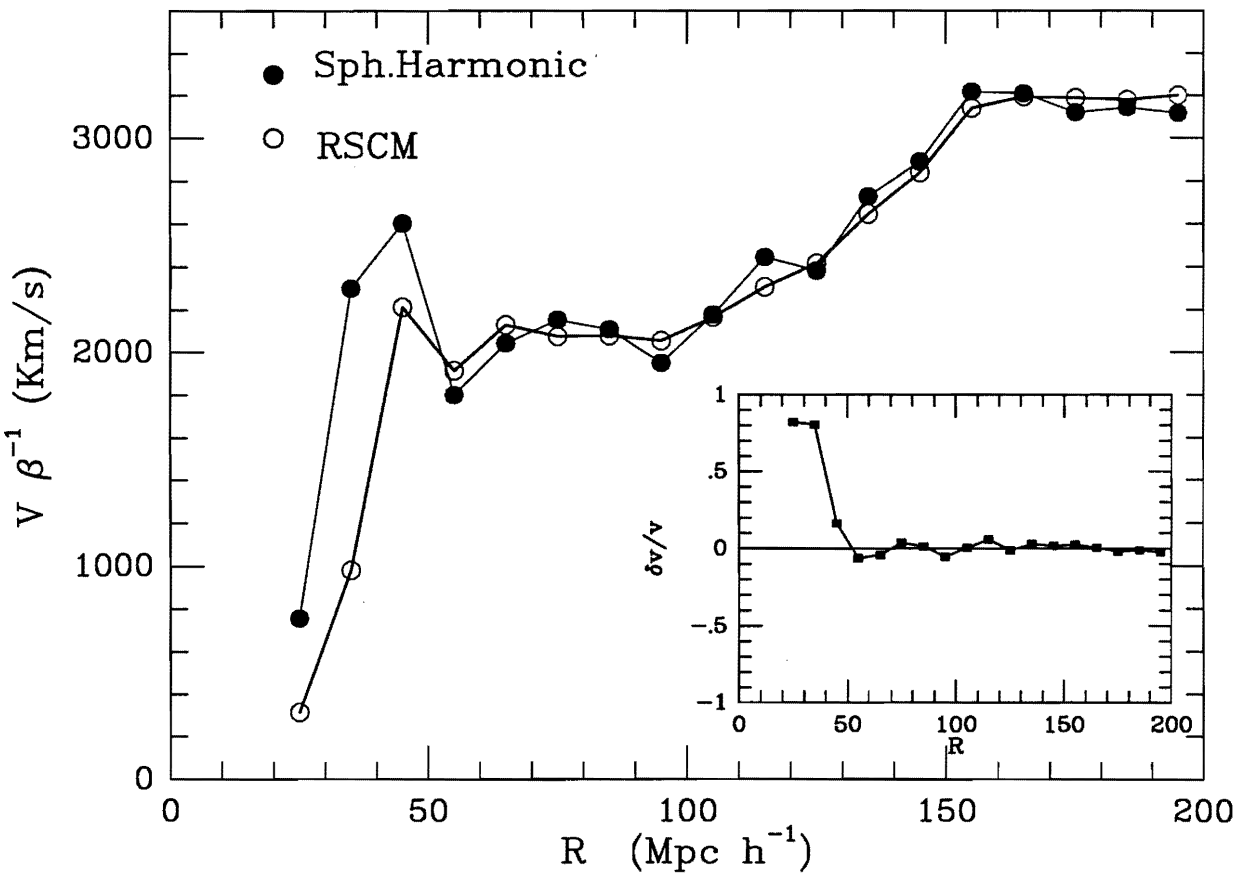
Sph.Harmonic
RSCM
V β^{-1} (Km/s)
R (Mpc h^{-1})
0
1000
2000
3000
0
50
100
150
200
$\delta v/v$
1
.5
0
−.5
−1
R

fig 6